AIAA AVIATION Forum
5-9 June 2017, Denver, Colorado
8th AIAA Theoretical Fluid Mechanics Conference

Optimal spatial growth of streaks in oblique shock/boundary layer interaction

Anubhav Dwivedi*, Joseph W. Nichols†, Mihailo R. Jovanovic*‡ and Graham V. Candler§
University of Minnesota, Minneapolis, MN, 55455, USA
* *University of Southern California, CA, 90089-2560, USA*

Direct numerical simulation (DNS) of oblique shock interacting with an incoming laminar boundary layer on an adiabatic flat plate at Mach 5.92 is considered. Various shock angles are considered to simulate interactions at various strengths. Above a critical shock angle, the flow around the separation bubble becomes three dimensional and transition to turbulence ensues. Previous studies[5,11] point to the existence of three-dimensional streak like structures just before transition occurs. In order to investigate the origin and the linear amplification of steady streamwise structures after the reattachment, we use an adjoint looping algorithm suitable for investigating spatial optimal growth. We modify this approach to account for the effect of curvature of streamlines due to the presence of the separation bubble. We further comment on the role of the non-modal spatial growth in transition due to such an interaction. With this analysis we observe that the boundary layer downstream of reattachment can support significant growth. Furthermore, spanwise wavenumber of the optimal perturbation at the reattachment location matches quite well with the energetical spanwise scale observed in DNS for a range of shock angles.

I. Introduction

Flow configurations involving high speed flows over complicated geometries are important for many high speed applications. In such configurations, Shock Boundary Layer Interactions (SBLI) are ubiquitous. A sufficiently strong adverse pressure gradient from an oblique shock impinging on a boundary layer flow can cause the flow to separate from the wall. The resulting laminar separation bubble can quickly become three dimensional and may transition to turbulence near the reattachment point. This transitional interaction can lead to significant aerothermal loads, potentially resulting in vehicle failure. A fundamental understanding of the transition process under such conditions is extremely essential.

Many previous studies have focused on the origin of low frequency unsteadiness of fully turbulent SBLI.[4,6,10] However, experimental and flight conditions can involve transitional interactions. In such scenarios, a broad range of flow phenomena may appear before the flow transitions depending on the state of boundary layer at the shock impingement location. A transitional boundary layer interacting with a shock may contain features of both fully turbulent and fully laminar interactions. Detailed experimental investigation by Schülein[15] considered a two dimensional shock wave impinging on a transitional boundary layer developing on a flat plate in a Mach 6 Ludwieg-Tube facility. Recent work by Sandham *et al.*[11] focuses on characterizing the effect of intermittancy of the transitional boundary layer on shock interactions. Further, they attribute the transition process in this scenario to develop from the second (Mack) mode instabilities superimposed on streamwise streaks. It is interesting to note that these experimental and computational studies have considered facilities with presence of significant free-stream acoustic disturbances.

Laminar interactions have been considered in numerous theoretical and computational studies as well. These interactions typically lead to large separated zones compared to fully turbulent or transitional interactions. The experimental studies by Hakkinen *et al.*[35] along with the triple deck analysis by Stewartson and

*Graduate Research Assistant, Aerospace Engineering and Mechanics, AIAA Student Member.
†Assistant Professor, Aerospace Engineering and Mechanics
‡Professor, Electrical Engineering
§Russell J. Penrose and McKnight Presidential Professor, Aerospace Engineering and Mechanics, AIAA Fellow.

Williams[38] have provided a detailed analysis of the laminar recirculation bubble. However, many aspects of transition in those configurations remains to be investigated. In this context linear stability analysis of the resulting flow field can provide some insight. For boundary layers with freestream Mach number above ~ 3, the transition process is dominated by the second Mack modes.[27,32,39] In SBLI configurations, the presence of a separation bubble leads to an additional source for disturbance amplification due to the separated shear layer. Pagella *et al.*[9] investigated the relevance of linear growth for small disturbances in flow over a ramp at Mach 4.8. Further work by Yao *et al.*[41] investigated the role of varying Mach number on the growth rate of linear stability modes for SBLI. Benay *et al.*[1] carried out numerical and experimental investigations for transition on a hollow cylinder flare. For shock impingement on a fully laminar boundary layer, they notice the presence of three dimensional organization of the flow field which was attributed to the presence of Görtler instability. However, the authors do not implicate Görtler vortices in the transition process observed downstream. It should be noted that all of these studies carried out a local linear stability analysis which treated the separated and attached parts of the boundary layer as independent and all the non-parallel effects were neglected. Recently, Robinet[7] considered oblique SBLI at Mach 2.15 by evaluating the growth rate of spanwise periodic two dimensional global instabilities. This allowed investigation of the global effect of separated and attached parts of the flow field on growth of small fluctuations. In fact it was shown that the three dimensonality of the resulting separation bubble in the DNS can be traced to the global linear instability of the two dimensional laminar base flow. However, due the low Reynolds number of the boundary layer no transition was observed even for very strong interactions. More recently, a study by Shrestha *et al.*[5] considered the interaction of oblique shock impinging on a laminar boundary layer at Mach 5.92, without free stream disturbances. For the higher Reynolds number considered in this study, the direct numerical simulation (DNS), produces streamwise streaks prior to transition. Further, these structures were observed to be almost steady. By comparing the results from DNS with the structure of the spanwise periodic two dimensional global modes, these streaks were proposed to originate from global linear instabilities.

It is interesting to note the presence of spanwise periodic three dimensional flow structures in all these laminar interactions before the flow transitions. In this context, numerical computations by Martinez & Tutty[33] investigated the growth and development of Görtler vortices in hypersonic compression ramps. Both the forced and natural development of spanwise periodic and steady structures was observed in these simulations. A large value of the Görtler number was cited as the reason for the development of these spanwise structures. However, there was a significant discrepency between the heat flux from the numerical computations and the experiments. Experiments by Bleibens & Olivier[2] report the presence of spanwise periodic structures near the reattachment location on a heated ramp model at Mach $\sim 7-8$. Recently, Yang *et al.*[40] carried out experiments at Mach 5 on a double ramp configuration. Techniques using temperature sensitive and pressure sensitive paint were used to characterize the location and properties of the three dimensional patterns near reattachment location. However, it should be noted that in most of these studies the comparison with theory on Görtler instability is only qualitative. A more detailed understanding of the role of centrifugal instability needs to be investigated to obtain a clear picture of its potential role in the emergence of three dimensionality and the process of transition.

Recent works by Reshotko[37] and many others, have commented that transition due to linear instability may only be one of the several routes for transition to turbulence. In this context, transient growth and non-modal amplification of stochastic and deterministic disturbances can play a very important role.[23,24] This is particularly important in situations where the growth has to occur within finite time and/or finite distance in space. Transient growth in both compressible[17,18] and incompressible[16,30] boundary layers has been extensively investigated by various researchers in the past. An adjoint based analysis by Cossu *et al.*[3] characterizes maximum spatial growth of Görtler vortices in an incompressible flow over concave walls. This work clearly illustrates the importance of non-modal nature of the boundary layer equations even in the presence of a centrifugal instability. A similar optimization based approach for investigating transient growth in space has been successfully applied to laminar separation bubble in the incompressible regime.[19]

In the present work, we consider the interaction of oblique shock wave with an incoming laminar boundary layer over an adiabatic flat plate at Mach 5.92. No external forcing in the free stream is assumed. DNS with a range of shock wave angles are considered to investigate the effect of increasing interaction strength. The three dimensional aspects of the flow field observed in these interactions are characterized. Further, in order to investigate the role of centrifugal instabilities in the origin of three dimensionality, spatial growth in the reattached portion of the two dimensional flow field is considered. An optimization procedure using the adjoints is proposed to obtain possible growth of streamwise steady and spanwise periodic perturbations in

the region after the reattachment location. The analysis allows us to investigate the role of algebraic growth of Görtler like vortices. Comparison of the results from this simplified analysis with the DNS is made to shed some light on their contribution to three dimensional flow field.

II. Numerical Setup and Flow Geometry

The focus of the current work is to understand the physical mechanism responsible for the generation of streamwise steady and spanwise periodic structures. In order to investigate the origin through numerical simulation we carry out a DNS of the oblique SBLI with a laminar boundary layer. The next few subsections briefly discuss the flow geometry and numerical method used to simulate the interaction. For more details reader is referred to our previous work.[5]

A. Numerical Scheme

We solve the compressible Navier-Stokes equations for a perfect gas in conservative form

$$\frac{\partial U}{\partial t} + \frac{\partial F_j}{\partial x_j} = \frac{\partial F_j^{\mathrm{v}}}{\partial x_j}, \tag{1}$$

where the vector of conserved variables U is

$$U = \begin{bmatrix} \rho \\ \rho u_i \\ E \end{bmatrix} \tag{2}$$

and the convective F_j and viscous F_j^{v} fluxes are expressed as

$$F_j = \begin{bmatrix} \rho u_j \\ \rho u_i u_j + p\delta_{ij} \\ (E+p)u_j \end{bmatrix}, \qquad F_j^{\mathrm{v}} = \begin{bmatrix} 0 \\ \sigma_{ij} \\ \sigma_{ij}u_i - q_{ij} \end{bmatrix}. \tag{3a,b}$$

The fluid density ρ and temperature T are related to pressure p through the equation of state for an ideal gas given by $p = \rho RT$. In the above equations, u_i is the i^{th} component of velocity and $E = \rho c_v T + \rho u_i u_i/2$ is the total energy. The viscous flux tensor σ_{ij} is defined as $\sigma_{ij} = 2\mu S_{ij} - 2\mu S_{kk}\delta ij/3$, where S_{ij} is the symmetric part of the velocity gradient tensor. We use Fourier's law to calculate the heat flux vector q_j. Molecular viscosity μ is calculated using Sutherland's law: $\mu = aT^{1.5}/(T+b)$ with $a = 1.458 \times 10^{-6}$ and $b = 110.4$. Finally, the thermal conductivity $k = \mu c_p/Pr$ is computed with a constant Prandtl number $Pr = 0.72$ and ratio of specific heats $\gamma = 1.4$.

For the inviscid flux calculation, we implement a stable low-dissipation scheme based on the Kinetic Energy Consistent (KEC) method developed by Subbareddy and Candler.[20] In this method, the inviscid flux is split into a symmetric (non-dissipative) and an upwind (dissipative) portion. The flux is pre-multiplied by a shock-detecting switch, ensuring that the dissipation occurs only around shocks.[21] We use a spatially sixth-order accurate central KEC scheme for the present study. Note that the viscous fluxes are modeled with second-order central differences.

Here time integration is performed using an implicit second-order accurate Euler method with point relaxation to maintain numerical stability and accuracy. The implicit system is also solved with the full matrix Data Parallel Point Relaxation (FMPR) method, which has good parallel efficiency.[25,26]

B. 2D Computations

We consider a laminar boundary layer at $M_\infty = 5.92$ with a unit Reynolds number equal to 4.6×10^6 m^{-1}. The free-stream temperature and pressure are $T_\infty = 53.06$ K and $p_\infty = 308.2$ Pa, respectively. These conditions match the experiments performed in the ACE Hypersonic Wind Tunnel[22] at Texas A&M University. A schematic representation of the domain used in the current work is shown in Figure 1. An incoming laminar boundary layer, with a displacement thickness, δ^* is shown. This inflow boundary layer for simulating the oblique SBLI is computed separately. A computation of zero pressure gradient boundary layer flow over a flat plate with a cylindrical leading edge ($r = 10^{-4}$ m) was carried out. For more details the reader is referred

to our previous study.[5] The boundary layer displacement thickness, δ^* is 2.1×10^{-3} at the inflow. All the length scales in the current work are non-dimensionalized using this as the length scale. The oblique shock at a shock angle, θ is generated at the inflow using Rankine-Hugoniot jump conditions. The oblique shock impinges the flat plate at $119\delta^*$ from the inflow for all the shock wave angles considered in the current work. This allows us to consider interaction at a fixed Reynolds number. The interaction of the oblique shock with the laminar boundary layer causes it to separate, eventually reattaching downstream. This results in separation bubble with a length X_{sep}. This changes with the strength of the interaction. The total length of the domain in the streamwise direction is $238\delta^*$. We implement an adiabatic wall at the bottom boundary and supersonic outlet along the right boundary.

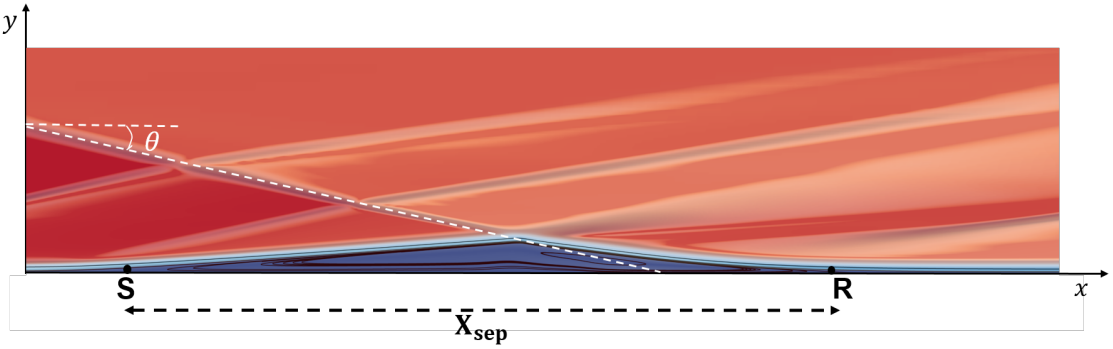

Figure 1: Domain for the oblique SBLI considered in the current work. The contours of streamwise velocity along with the density gradient magnitudes are shown. The streamlines within the boundary layer and the recirculation bubble along with the separation point, S and the reattachment point, R are also marked.

To accurately capture the gradients we use a stretched grid along the wall normal direction with the near-wall $y^+ = 0.5$. Here, y^+ is the non-dimensional distance in viscous units. Uniform mesh spacing is chosen in the streamwise direction to resolve the small wavelengths of the traveling waves in the streamwise direction. A grid convergence study was carried out and showed that $n_x = 998$ points in the streamwise along with $n_y = 418$ points in the wall normal direction are sufficient to resolve the two-dimensional flow field. In the present study, four shock angles are considered in order to investigate the effect of interaction strength in oblique SBLI. Two dimensional computations of oblique SBLI at shock angles, $\theta = 12.0°, 13.0°, 13.6°, 14.0°$ are considered. Figure 2 shows the contours of Mach number and pressure for one such computation carried at $\theta = 13°$ in a two dimensional domain. Please note that all the two dimensional computations for all shock wave angles considered are steady.

Figure 3 shows the variation of skin friction coefficient at the wall for all shock wave angles considered. This is helpful in obtaining a quantitative estimate of the extent of separation with varying interaction strengths. The separation bubble corresponds to the region of the flow with negative skin friction coefficient. It is interesting to note that, for increasing shock angles the reattachment point remains relatively fixed while the separation point moves upstream (see angles, $\theta \geq 13°$). Also, increasing the interaction strength leads to emergence of small regions (secondary bubble) with positive skin friction coefficient within the larger region of negative skin friction coefficient (primary bubble). This starts to appear for interaction at $\theta = 13.6°$ and can be seen clearly for $\theta = 14°$.

C. 3D Simulations

In order to simulate any 3D effects which might originate due to SBLI, 3D computations are carried out for all the shock interactions considered in the present study. The computations are initialized using the two-dimensional flow field corresponding to the oblique SBLI at the corresponding shock wave angle. The 2D domain is extruded in the spanwise direction and periodic boundary conditions are enforced. Ideally, the spanwise length should be as large as possible for three dimensional instabilities to appear spontaneously.[7] In the present case, it was found that a spanwise length of $95.2\delta^*$. It was found that 200 uniformly distributed points are sufficient to resolve the three dimensional phenomena of interest. In the present study no external forcing is introduced in the flow field. It is found that the flow field for $\theta = 12°$ remains two dimensional

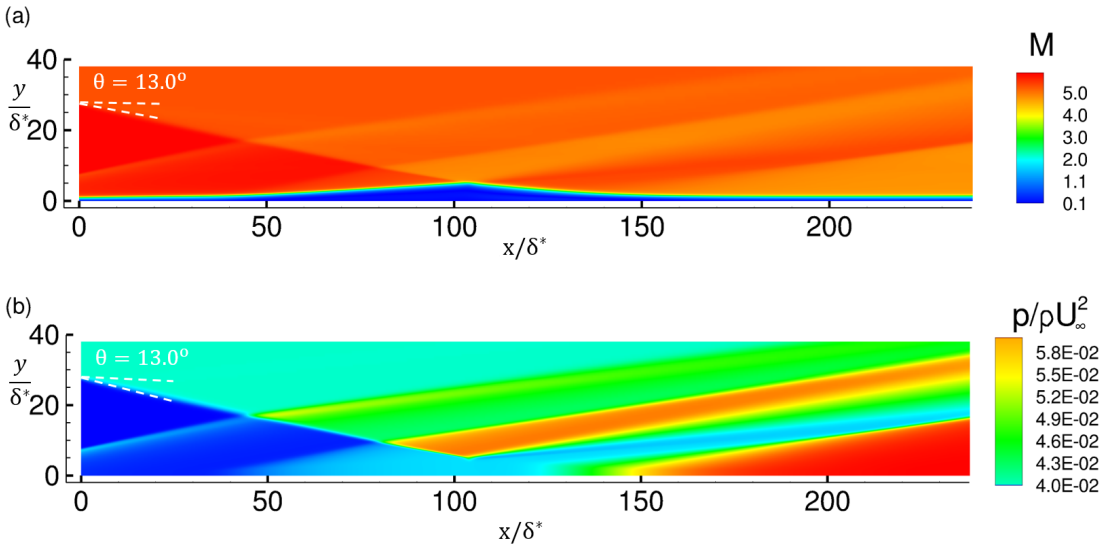

Figure 2: (a) Mach number and (b) Non-dimensionalized pressure contours for SBLI at $\theta = 13°$. The weak oblique shock at the inflow is the bow shock from the leading edge of the flat plate.

even after integrating for more than 80 flow through times. On the other hand, at $\theta = 13°$ the flow field starts becoming three dimensional after about 15 flow through times. However, no unsteadiness is noticed in the resulting flow field. For stronger interaction at $\theta = 13.6°$ and $\theta = 14°$, we notice the flow field quickly becomes 3D (after about 15 flow through times). It eventually becomes unsteady inside the recirculation bubble and near the reattachment location. After a sufficiently long time, we start to notice that the attached boundary layer transitions. Figure 4 shows the snapshot of the spanwise velocity for $\theta = 13.0°, 13.6°, 14.0°$ after 80 flow through times.

In order to investigate the spatio-temporal characteristics of the resulting flow field. We compute time averaged Power Spectral Density (PSD) of the streamwise velocity fluctuations. Spanwise snapshots were taken at a fixed interval of $20\mu s$ $(0.035L/U_\infty)$ for about 21 flow through times (605 snapshots). Figure 5 shows the time averaged power spectral density for $\theta = 13°, 13.6°, 14.0°$. For $\theta = 13°$ we can see the emergence of a relatively few length scales in the spanwise drection. We notice a maximum at a spanwise wavenumber, $\beta\delta^* = 0.24$, which corresponds to roughly 3 wavelengths in the spanwise direction. This length scale is energetically dominant within the bubble but then quickly decays in the region near reattachment. However, it appears again in the region after reattachment towards the end of domain where it persists for a significant distance in the downstream direction. Thus, pointing to the spatial amplification of steady spanwise periodic streamwise velocity fluctuations in the reattaching boundary layer. Local maxima corresponding to the higher harmonics are also present. At $\theta = 13.6°$, apart from a local maximum at $\beta\delta^* = 0.24$, we note the presence of several other spanwise periodic fluctuations corresponding to its higher harmonics. Further, most of these higher harmonics grow downstream close to the reattachment location. For $\theta = 14°$, the peak in $\beta\delta^*$ vanishes. The energy is distributed continuously over a range of spanwise wavenumbers. We notice the emergence of two new peaks at $\beta\delta^* = 0.87$ and $\beta\delta^* = 1.20$. Even though the flow field still exhibits the presence of several spanwise periodic structures, we notice the presence of significantly higher levels of flow unsteadiness inside the bubble and near the reattachment location.

III. Centrifugal Instabilities

Observations from the DNS at various interaction strengths point to the presence of steady spanwise periodic fluctuations within the separation bubble and reattached boundary layer. Further, large and rapid amplification of the streamwise fluctuations is observed in the reattached boundary layer. Previous studies involving laminar SBLI on compression ramps have commented on the role of Görtler instability for the emergence of these streak like steady structures.[1,33] In this context, it is interesting to note that separation

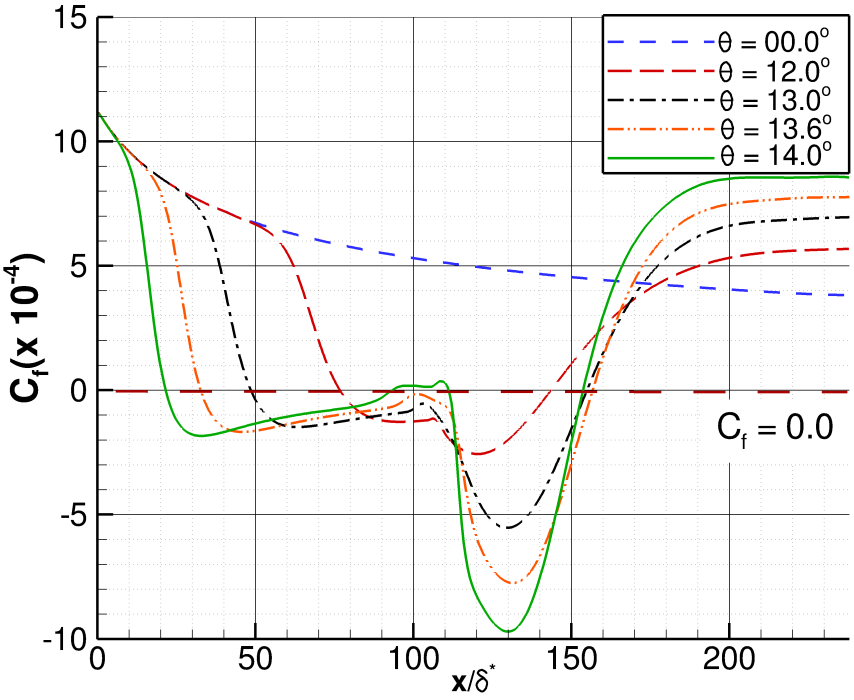

Figure 3: Skin friction distribution for various shock interaction strengths. The variation of skin friction coefficient in the absence of any oblique shock is also plotted for comparison.

bubble introduces curvature in the streamlines near the reattachment and the separation location. The curvature of streamlines can lead to the presence of Görtler like centrifugal instabilities in these regions. One way to quantify possible regions of growth due to this is to consider the variation of Görtler number along the streamwise direction. In the present work, the Görtler number is defined as,

$$Ge^2 = \frac{U_\infty L \delta}{\nu \mathcal{R}} \tag{3}$$

Here, L, denotes the reference length (taken to be the streamwise distance) and δ denotes the boundary layer thickness. Further, $\mathcal{R}$ denotes the radius of curvature of the streamline; we calculate $\mathcal{R}$ along the separation streamline. Figure 6 shows the variation of the Görtler number for all shock angles considered. Note that only real and positive values of the Ge have been shown. Previous work on Görtler instability in compressible flows on curved walls have shown that the critical value for Görtler instability to become important for $Ge \sim 0.6$.[28] This value along with the separation and the reattachment points are marked in Figure 6. For weaker interactions $\theta = 12°$, the streamwise variation of Ge is symmetric near both the reattachment and the separation point. Further, we notice finite regions of the flow near separation and reattachment points, which are locally unstable to centrifugal instabilities. It is interesting to note that despite this, DNS shows no three dimensionality. For larger shock wave angles we notice that the spatial variation of Görtler number is no longer symmetric. This asymmetry shows up as a larger value of Ge near the reattachment location. Increasing the shock wave angle, increases this asymmetry, with the value of Görtler number remaining reasonably constant near the separation point. However, unlike flow on curved walls which often involves constant or slowly varying wall curvature, we note a rapid change in streamline curvature. This is important in the context of spatial growth of Görtler vortices, which now have to occur in boundary layer with a rapidly changing curvature. Further, the idea of defining a critical number based on local analysis is justified only when the boundary layer thickness is large compared to the spanwise wavelength of the Görtler vortices.[29] Thus, to investigate the possible growth we need a methodology for computing disturbance growth which takes into account this rapid variation of streamline curvature after

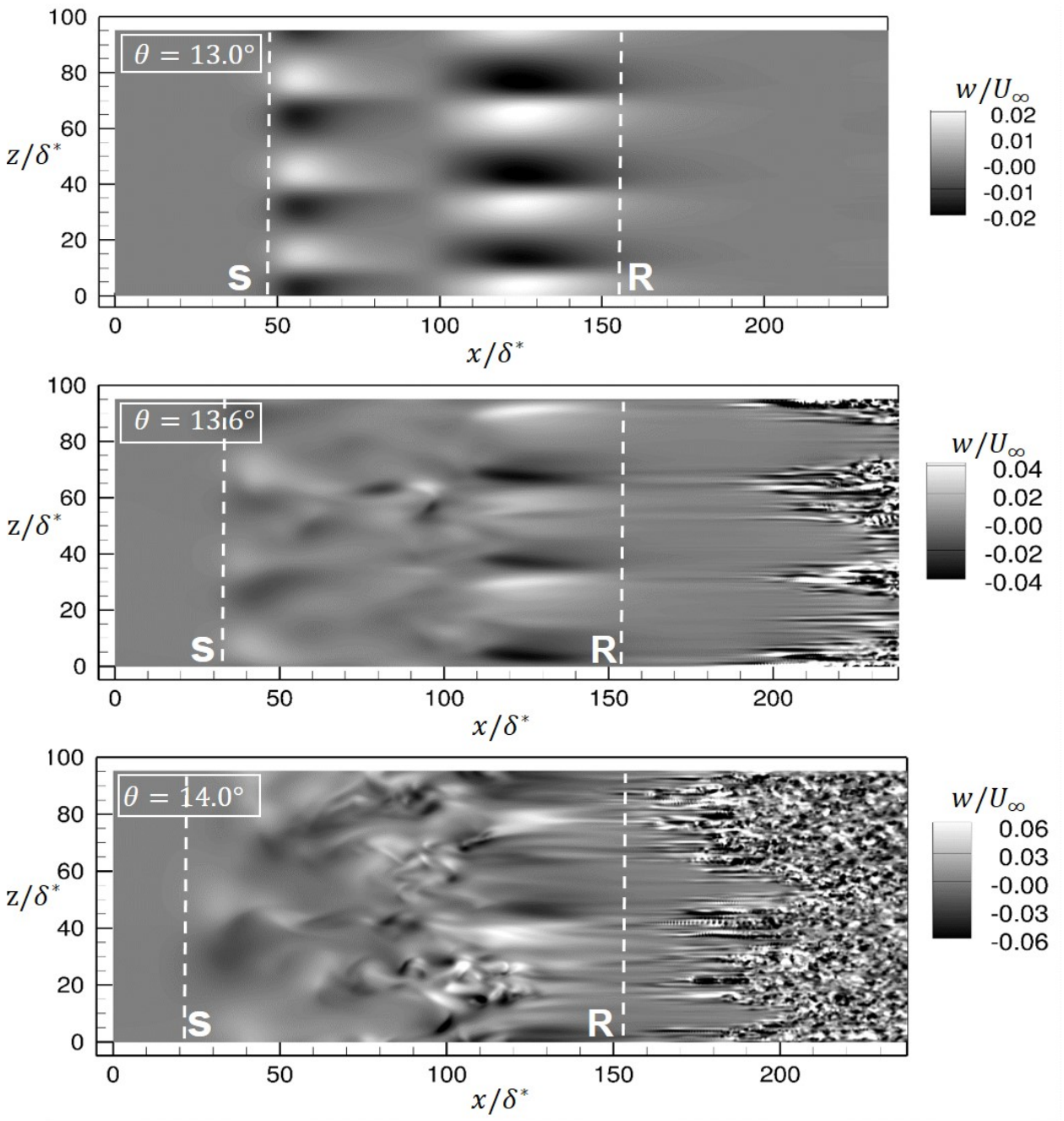

Figure 4: Snapshot of spanwise velocity fluctuation for (a) $\theta = 13°$, (b) $\theta = 13.6°$ and (c) $\theta = 14.0°$. The data are collected at wall normal distance of $y/\delta^* = 1$. The points S and R denoting the separation and reattachment locations are also marked.

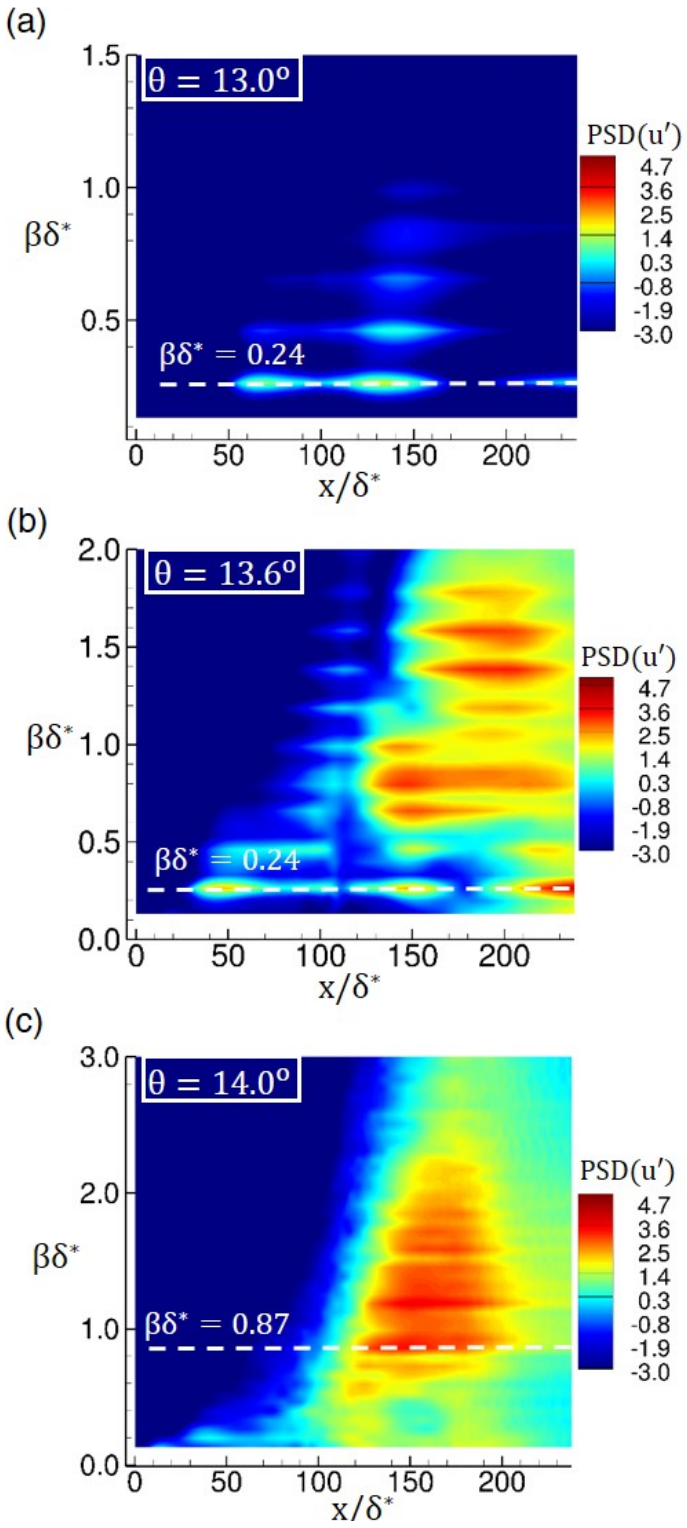

Figure 5: Power spectral density of streamwise velocity fluctuations at various streamwise locations for (a) $\theta = 13°$, (b) $\theta = 13.6°$ and (c) $\theta = 14.0°$. The data are collected at wall normal distance of $y/\delta^* = 1$. Most energetic spanwise wavenumbers are also marked.

reattachment.

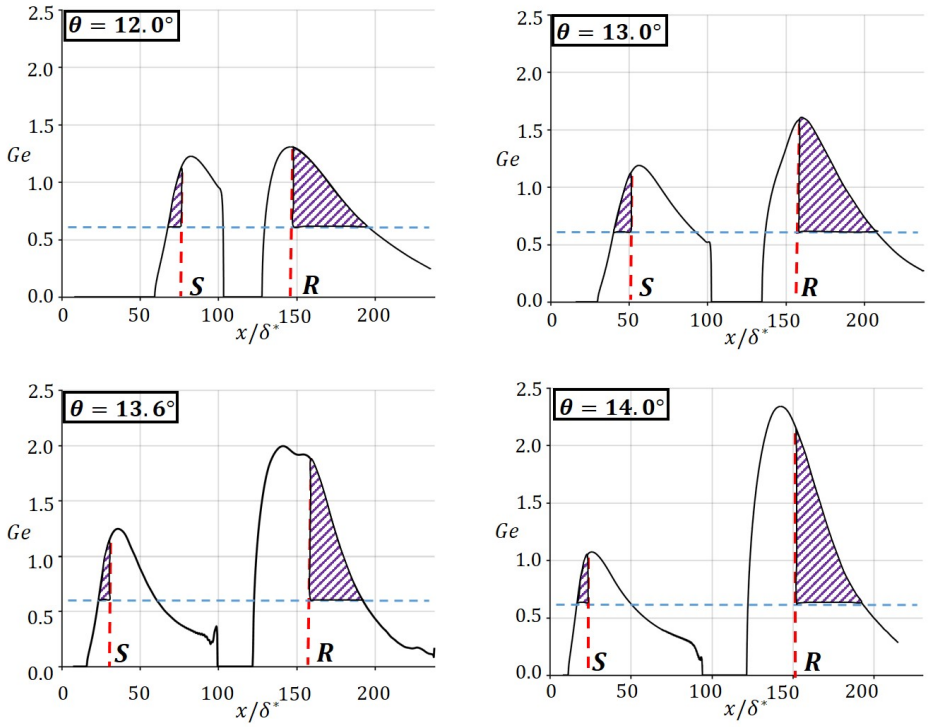

Figure 6: Streamwise variation of Görtler number for the separation streamline. The points S and R, denote the separation and the reattachment points. The shaded region denotes the attached portion of the flow which is locally unstable to Görtler instability.[28]

Previous work (especially on wedges[12,33]) has often focused on using the spatial variation of the Görtler number (Ge) as an indicator for the importance of the centrifugal instability. Any investigation of spatial growth due to centrifugal instability should also account for possible growth from non-modal effects. In the present work, we significantly simplify our analysis by restricting the attention to the attached portions of the boundary layer. In particular, the focus would be on finding the maximum possible growth in the attached portion of boundary layer after the reattachment point.

The role of transient growth of steady spanwise disturbances due to non-orthogonality of the eigenmodes in zero pressure gradient boundary layer flows has been extensively investigated.[13] Transient growth can also occur in space. Even though the growth occurs over a finite distance, the amplitude of growth can be considerably large. Previous work by Cossu *et al.*[3] has considered maximum growth associated with Görtler vortices on concave walls. In the next few sections, we briefly describe the methodology behind computing upper bound on spatial growth of Görtler vortices in compressible boundary layer. In the present work, we closely follow the work by Tumin *et al.*[17] for using an adjoint based iterative algorithm to calculate the inflow disturbances resulting in the largest gain in disturbance energy for a certain streamwise distance.

A. Transient Growth in Space

1. Linearized Boundary Layer Equation

In the current work we are interested in understanding the amplification property of the attached portion of the boundary layer downstream of reattachment. The observations from DNS suggest that these are steady elongated disturbances which are periodic in spanwise direction. In general, evolution of small perturbation in compressible flows is governed by linearized disturbance equation.[7,31] However, restricting our attention to reattached boundary layer, we can further simplify the linearized equations assuming the boundary layer scaling. We define the small parameter $\epsilon = Re^{-1/2} = \sqrt{\mu_\infty/(\rho_\infty U_\infty L)}$. Here, $U_\infty, \mu_\infty, \rho_\infty$ are the free stream speed, coefficient of dynamic viscosity and density respectively. Assuming that the streamwise coordinate

scales with a characteristic length, L along the flat plate, whereas the wall normal and spanwise coordinate scale with $\sqrt{\mu_\infty L/(\rho_\infty U_\infty)}$. Also,

$$\begin{aligned} u' \sim U_\infty \quad v' \sim \epsilon U_\infty \quad w' \sim \epsilon U_\infty \\ \rho' \sim \rho_\infty \quad \pi \sim \epsilon^2 \rho_\infty U_\infty^2 \quad \theta \sim T_\infty \end{aligned} \tag{4}$$

Here, $\{u', v', w', \rho', \pi, \theta\}$ denote the disturbance velocities, density, pressure and temperature, respectively, and T_∞ denotes the free stream temperature. Further, we assume that the disturbances are steady in time and periodic in the spanwise direction. In other words,

$$\phi(x, y, z) = \phi(x, y) e^{i\beta z} \tag{5}$$

Here, $\phi = (u', v', w', \theta, \pi)^T$ denotes the disturbance state vector and β denotes the spanwise wavenumber. Using the scaling from Equation 4 and the disturbance form given by Equation 5, the linearized disturbance equation can be simplified to

$$(\mathcal{A}\phi)_x = \mathcal{B}_0\phi + \mathcal{B}_1\phi_y + \mathcal{B}_2\phi_{yy} \tag{6}$$

Where, $\mathcal{A}, \mathcal{B}_0, \mathcal{B}_1, \mathcal{B}_2$ are all 5×5 matrices. The non-zero entries of these matrices are presented in the Appendix. This is the governing equation for Görtler instability in compressible boundary layer. The following boundary conditions are applied at the wall and the free stream :

$$\begin{aligned} u' = v' = w' = \theta = \frac{d\pi}{dy} = 0 \qquad \text{at} \quad y = 0 \\ u' = v' = w' = \theta = \pi = 0 \qquad \text{at} \quad y = y_{max} \end{aligned} \tag{7}$$

Equation 6 along with boundary conditions, 7 determine the downstream evolution of disturbance (Equation 5) starting from a given initial condition at location x_{in}.

2. Spatial Growth Optimization

The DNS shows that at the onset of three dimensionality for interaction at $\theta = 13°$ (see Figure 4) the spanwise velocity fluctuations appear as elongated structures in the streamwise direction but decay downstream of the reattachment location. Whereas, streamwise velocity fluctuations keep increasing as we go downstream (see Figure 5). This motivates us to investigate the growth of perturbations in the form of streamwise vortices at the reattachment point which develop into streamwise velocity fluctuation downstream. In order to obtain an upper bound on the possible growth, we wish to identify the disturbance pattern (with unit energy) at reattachment point which maximizes the energy at the downstream plane at x_{out}.

First, we need to choose a measure for energy of disturbances in compressible flows. In general, the energy of a perturbation (within the scope of parallel flow) can be described by the following norm,[32,36]

$$2\mathcal{E} = \int_0^\infty \boldsymbol{\phi}^H \boldsymbol{\mathcal{M}} \boldsymbol{\phi} dy \tag{8}$$

Here,

$$\boldsymbol{\mathcal{M}} = \mathrm{diag}\Big(\frac{\bar{T}}{\bar{\rho}\gamma M^2}, \bar{\rho}, \bar{\rho}, \bar{\rho}, \frac{\bar{\rho}}{\gamma(\gamma-1)\bar{T}M^2}\Big)$$

Note that the base flow quantities are denoted as, $\bar{\rho}, \bar{U}, \bar{V}, \bar{T}$. The objective of optimization can be written as maximization of the ratio $\mathcal{E}(x_r)/\mathcal{E}(x_{out})$ for various initial conditions. Here, x_r is the reattachment location and x_{out} is the downstream location where the maximum of the growth is sought. However, assuming the scaling of the disturbances described above and the form of the disturbances observed in the DNS, we can simplify the expression for energy at the reattachment, x_r for streamwise vortical disturbances as,

$$\mathcal{E}_{x_r} = \int_0^\infty [\bar{\rho}(v^2 + w^2)] dy \tag{9}$$

Similarly, at the downstream location, the expression for energy simplifies by considering only the contribution from the streamwise and temperature perturbation. Using the equation of state we obtain the following,

$$\mathcal{E}_{x_{out}} = \int_0^\infty [\bar{\rho}u^2 + \frac{\theta^2}{(\gamma-1)\bar{T}^2M^2}]dy \tag{10}$$

The optimization procedure now maximizes the energy ratio defined by Equations 10 & 9. A power iteration algorithm using the forward equations (Equation 6) and the adjoint equation is employed.[16,17,30] Using the approach suggested by[13,17] the adjoint variable, ψ satisfies the following adjoint equation,

$$-\mathcal{A}^H\psi_x = \mathcal{B}^H\psi - (\mathcal{B}_1^H\psi)_y + (\mathcal{B}_2^H\psi)_{yy} \tag{11}$$

The boundary conditions are given by:

$$\begin{aligned} \psi_2 = \psi_3 = \psi_4 = \psi_5 = 0 \qquad \text{at} \quad y = 0 \\ \psi_1 + \psi_2 + 2\bar{V}\psi_3 + \psi_5 + (4/3)(\psi_3)_y = 0 \qquad \text{at} \quad y = y_{max} \end{aligned} \tag{12}$$

Note that the adjoint equations are well posed in the direction opposite to forward linearized boundary layer equations. Hence, they are solved backwards from x_{out} to x_r. To do that we initialize the adjoint modes ψ at x_r using the following equations,

$$\begin{aligned} \psi_1(x_{out}) = \frac{-1}{\bar{\rho}^2\bar{U}}\frac{\phi_4}{(\gamma-1)(\bar{T}M)^2}\Big|_{(x_{out})} \\ \bar{\rho}(x_{out})\psi_1(x_{out}) + \psi_5(x_{out}) = \bar{\rho}(x_{out})\phi_1(x_{out}) \\ \psi_2(x_{out}) = \psi_3(x_{out}) = \psi_4(x_{out}) = 0 \end{aligned} \tag{13}$$

Here, $(\phi_1, \phi_2, \phi_3, \phi_4, \phi_5)^T = (u, v, w, \theta, \pi)^T$ and the over bar denotes the base quantities.

After integrating backwards to x_r we solve the forward equations again (Eq. 6) with the following initial conditions:

$$\begin{aligned} \phi_1(x_r) = \phi_4(x_r) = 0 \\ \phi_2(x_r) = \bar{U}(x_r)\psi_3(x_r) \\ \phi_3(x_r) = \bar{U}(x_r)\psi_4(x_r) \end{aligned} \tag{14}$$

The ϕ at the inflow, (x_r) is then scaled such that $\mathcal{E}_{x_r} = 1$. This process of iteratively solving the forward and the adjoint equation is carried out until the growth ratio, $\mathcal{E}_{x_{out}}/\mathcal{E}_{x_r}$ converges. This is shown schematically in Figure 7. Further details regarding the derivation of these equations can be found in the appendix of the work by Tumin *et al.*[17]

B. Numerical Procedure

Both the forward equations and the adjoint equations are discretized using Chebyshev polynomials.[13] The wall normal two dimensional base flow is interpolated to a set of Gauss-Lobatto points. The presence of discontinuities is neglected and only the base flow properties within the attached boundary layer are considered for interpolation. Since the governing equation is assumed to be parabolic, a second order implicit scheme is used to march the solution in the streamwise direction.[16] For Equation 6 this can be written as

$$\begin{aligned} \frac{3}{2}(\mathcal{A}\phi)^{n+1} - 2(\mathcal{A}\phi)^n + \frac{1}{2}(\mathcal{A}\phi)^{n-1} = \frac{3}{2}\Big(\mathcal{D}\frac{\partial\phi}{\partial y}\Big)^{n+1} - 2\Big(\mathcal{D}\frac{\partial\phi}{\partial y}\Big)^{n} + \frac{1}{2}\Big(\mathcal{D}\frac{\partial\phi}{\partial\phi}\Big)^{n-1} \\ +\Delta x\Big[(\mathcal{B}_0\phi)^{n+1} + \Big(\mathcal{B}_1\frac{\partial\phi}{\partial y}\Big)^{n+1} + \Big(\mathcal{B}_2\frac{\partial^2\phi}{\partial y^2}\Big)^{n+1}\Big] \end{aligned} \tag{15}$$

Here, n denotes the *nth* streamwise station. For the first step however, implicit Euler is used

$$(\mathcal{A}\phi)^1 - (\mathcal{A}\phi)^0 = \Big(\mathcal{D}\frac{\partial\phi}{\partial y}\Big)^1 - \Big(\mathcal{D}\frac{\partial\phi}{\partial y}\Big)^0 + \Delta x\Big[(\mathcal{B}_0\phi)^1 + \Big(\mathcal{B}_1\frac{\partial\phi}{\partial y}\Big)^1 + \Big(\mathcal{B}_2\frac{\partial^2\phi}{\partial y^2}\Big)^1\Big] \tag{16}$$

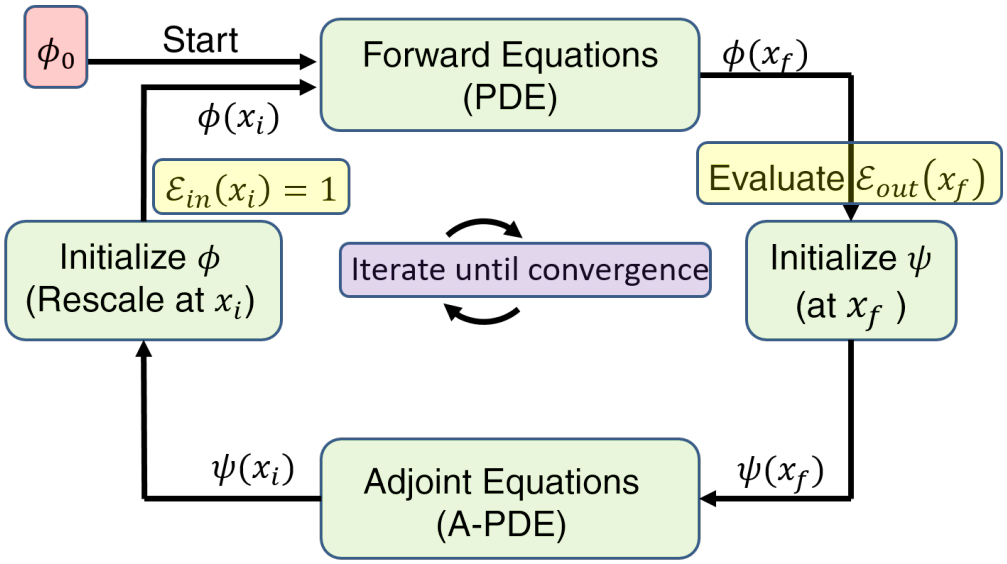

Figure 7: A sketch of the iterative scheme for finding maximum growth for steady spanwise periodic perturbations at outflow location, x_{out} starting from an initial vortical perturbation at reattachment location, x_r.

Here, Δx denotes the size of the step along the streamwise direction. In the present case this value is taken to be the same as the one used in the base flow calculations. Using a value of $\Delta x/2$ does not have any effect on the results. Similarly, the adjoint Equation 11 is integrated in the backward direction using the same numerical scheme. It is found that 450 points in the wall normal direction are sufficient to produce grid independent results.

C. Spatial Optimal Growth

In order to obtain an upper bound on the growth of the Görtler like vortices, we restrict our attention to the reattached portion of the boundary layer. The optimization procedure discussed in the previous section involving the use of forward linearized boundary layer and backward adjoint equations is used. Note that the effect of centrifugal instabilities due to curvature of the streamlines near the reattachment point is taken into account by using the previously defined values of the Görtler number (see Figure 6).

Figure 4 shows the variation of maximum growth of perturbations with various spanwise wavenumbers starting from the reattachment point. In the optimization procedure discussed earlier, the initial location is kept fixed at the reattachment location. On the other hand, the final location is taken as a parameter. This is important because for a given streamwise extent from the reattachment location we are optimizing over all possible initial conditions with a unit energy norm. These initial condition may be different for different downstream locations. We can see from Figure 8 that the value of growth that is possible over a finite distance increases as we go further downstream for all the interactions considered. This shows us that the flow after the reattachment is in fact centrifugally unstable. Further, it is interesting to note the differences in the possible growth among various shock wave angles. For weaker interaction at $\theta = 12.0°$, we notice a band of wavenumbers, $\beta \sim 0.18 - 0.26$ with a maxima around $\beta = 0.22$ can show significant growth. As we keep increasing the strength of interaction, for $\theta = 13.0°$, we notice a significant growth associated with a broader range of spanwise wavenumbers. Also, larger growth is possible further upstream. Further, it is interesting to note that the wavenumber corresponding to maximum growth for $\theta = 13.0°$ occurs around $\beta = 0.24$. This is remarkably close to the value observed from the DNS (see Figure 5). Increasing the shock angle magnifies these trends further. For $\theta = 13.6°$ a much broader peak is observed along with a maxima around $\beta = 0.24$. The DNS (Figure 5) shows the peaks at $\beta \sim 0.24$ along with its higher harmonics near the reattachment location. For $\theta = 14°$ we again notice maximum growth around $\beta = 0.28$. However, this is not observed in the DNS. This may have to do with the fact that at such a large interaction strength, the bubble becomes significantly more unsteady and larger range of perturbations are active. In this context,

a simplified analysis which ignores the contribution from the bubble may not be useful. Further, we also notice a much broader range of wavenumbers with significant growth indicating that other wavenumbers might grow significantly within the boundary layer.

Using this analysis we can also comment on the relative importance of the algebraic (non-modal) and exponential (modal) interactions within the reattached boundary layer. Figure 8 shows the maximum of the growth for all spanwise wavenumber, β and the final downstream location using the optimization procedure described previously. This clearly shows that closer to the reattachment location algebraic growth dominates over the exponential growth. Moving further downstream, exponential growth plays an important role. Note, that the exponential effects start becoming more important at a streamwise location of $x/\delta* \sim 210$ for all the shock wave angles considered.

It is interesting to note the shape of the optimal perturbation which can lead to the maximum growth in these flows. Figure 10 shows the optimal input and the corresponding response. Starting with initial vortical disturbance (i.e. with only v' and w') we obtain a spatial growing streamwise velocity fluctuation. This observation clearly points to the important role played by the lift up effect even in the presence of centrifugal terms in the linearized bundary layer equation. A similar observation was reported for incompressible flow over the concave wall by Cossu *et al.*[3]

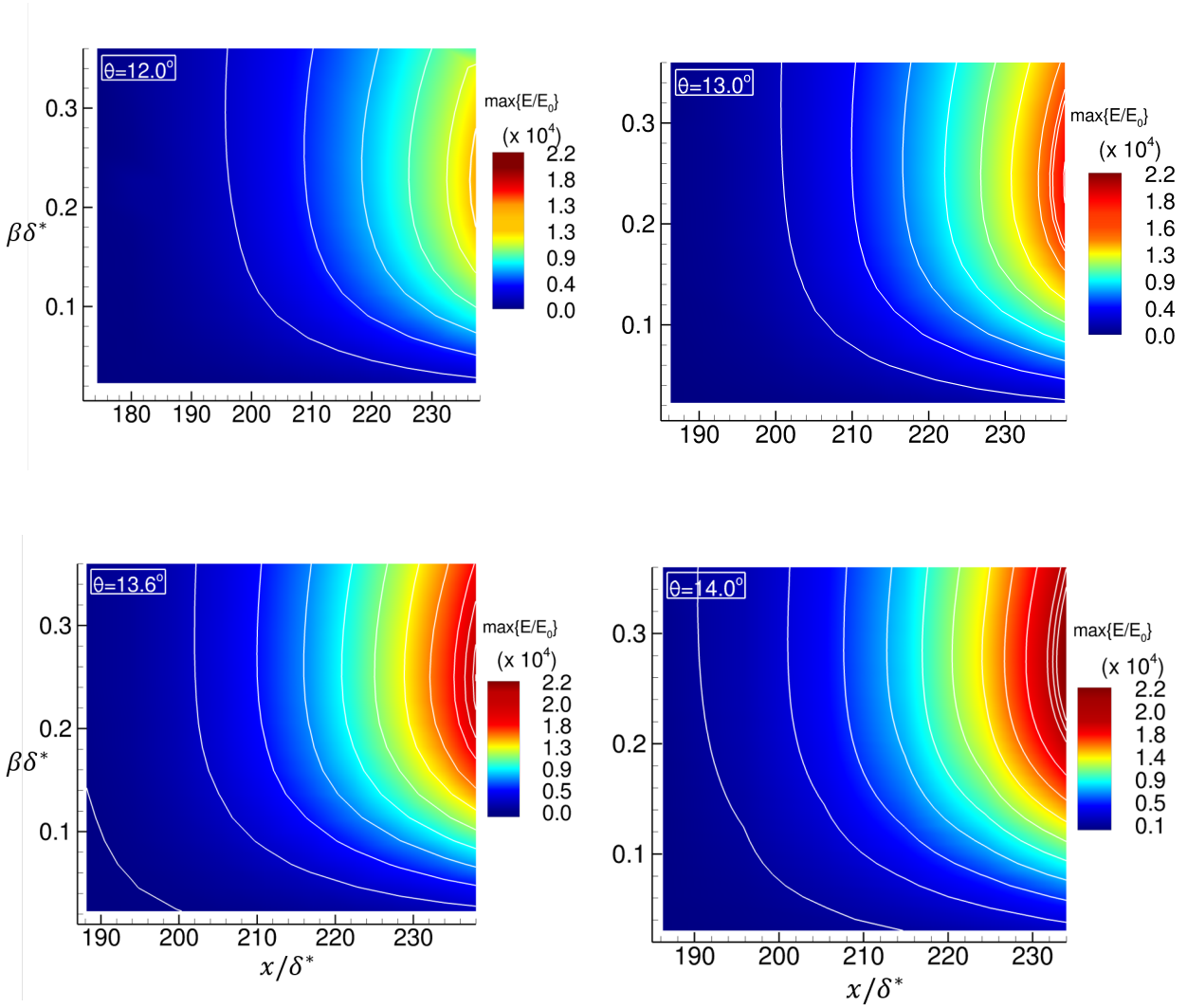

Figure 8: Maximum spatial growth in the boundary layer after reattachment for various spanwise wavenumber, β

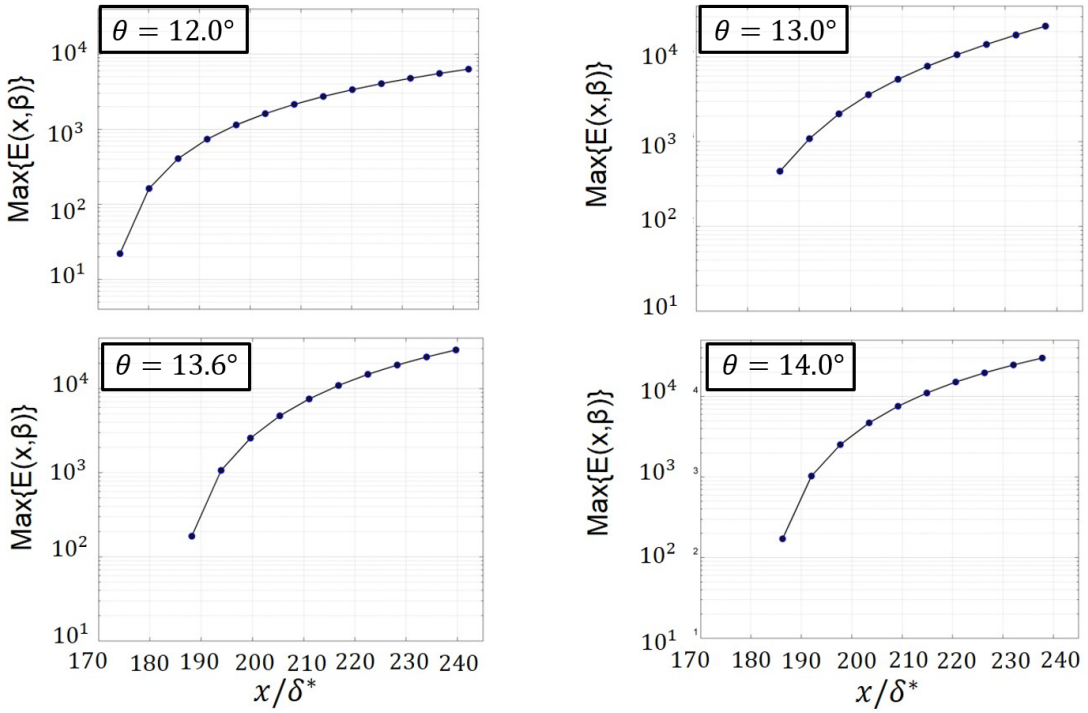

Figure 9: Maximum spatial growth in the boundary layer after reattachment, for various spanwise wavenumbers β and streamwise distance $x/\delta*$ for optimization

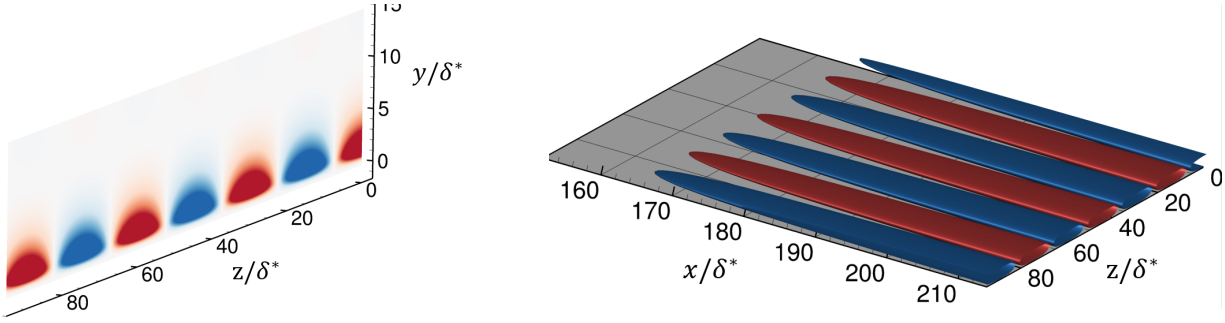

Figure 10: Shape of the optimal input fluctuation (contours of v' are shown) and the optimal response (isosurface of the u')

IV. Discussion and Conclusions

Direct Numerical Simulation (DNS) of oblique Shock Boundary Layer Interaction (SBLI) is carried out for various shock wave angles. An incoming laminar boundary layer over a flat plate at Mach 5.92 without the presence of any external perturbations is considered. For smaller shock wave angles, the flow remains two dimensional and steady. For stronger interactions, a steady three dimensional flow field emerges. This three dimensionality is characterized by the presence of streamwise structures which are periodic in span. An analysis of the spanwise Power Spectral Density (PSD) of streamwise fluctuations shows the presence of discrete wavenumbers, some of which are energetically more significant than others. Furthermore, we notice significant growth of streamwise fluctuations near and just downstream of the reattachment location. For $\theta = 13^\circ$ we note that a single spanwise wavenumber at $\beta = 0.24$ to be most dominant. Increasing the strength of interaction further, leads to emergence of more spanwise scales. The flow becomes unsteady near the reattachment location but most of the energy is still present in the spanwise scale with $\beta = 0.24$ and its higher harmonics. Within the bubble the flow becomes unsteady and the flow transitions further downstream after reattachment. For oblique SBLI at $\theta = 14.0^\circ$, the energy peak at $\beta = 0.24$ vanishes and higher spanwise wavenumbers become more energetically significant. It should be noted that for all of these interactions, the three dimensionality and the unsteadiness is confined to the separation bubble and the reattachment point whereas the separation line remains undisturbed.

Previous studies of SBLI[2, 12, 33] have suggested Görtler instability as the responsible mechanism for these structures. In order to investigate the role of centrifugal instability due to the curvature of the streamline at the separation and the reattachment location, we consider the distribution of the Görtler number for the various shock angles considered in the DNS. It is found that the Görtler number exceeds the critical value for instability in the regions near the reattachment location while remaining reasonably constant in the region near the separation point. In order to investigate the spatial growth of Görtler like perturbations over a finite distance in space we follow an approach proposed by Cossu *et al.*[3] This allows us to account for the non-modal algebraic growth of perturbations in space.[3, 16, 17] Using boundary layer scaling a parabolic system of equations governing the spatial evolution of Görtler vortices in compressible boundary layer is obtained. An adjoint based iterative approach is used to obtain the maximum growth of vortical spanwise periodic perturbation in the reattached part of the boundary layer. The analysis is carried out for various spanwise wavenumbers. It is found that for perturbations starting at the reattachment location there is continuous band of spanwise wavenumbers which can show significant growth downstream. The analysis also reveals that reattached boundary layer supports larger growth for a broader range of spanwise wavenumbers at stronger interactions than at weaker interactions at smaller shock angles. The shape of the initial of the initial perturbation which leads to maximum response downstream clearly shows the importance of lift-up in this interaction. Interestingly, even though we are completely neglecting the role played by the separation bubble, we do find that the spanwise wavenumber corresponding to the maximum growth is also seen in the DNS at moderate interaction strengths for oblique shock at $\theta = 13.0^\circ$ and $\theta = 13.6^\circ$.

From this analysis we can clearly see the important role played by centrifugal instability due to streamline curvature in promoting large growth in the regions after reattachment. There is also a close match between the optimal spanwise wavenumber and the energetically dominant spanwise scale in DNS. The role of separation bubble is however neglected in the current framework. The Biglobal linear stability analysis[5, 7] has shown the presence of global modes which lead to the three dimensional state in the numerical simulations. This is interesting in the context of many experimental configurations where wind tunnels often have non-negligible levels of free stream pressure fluctuations which the SBLI can amplify. The simplified analysis presented in the current work gives us some indications that an analysis of the forced response of the system might play an important role in understanding several aspects of this interaction.

V. Appendix

The base flow quantities are denoted as $(\bar{\rho}, \bar{U}, \bar{V}, \bar{T})$. Using the scaling given by Eq. 4, the equation of state for the perturbation is given as,

$$\rho = -\frac{\theta}{\bar{T}^2} \tag{17}$$

The governing equations for zero Görtler number are derived and given in Tumin.[17] In the current work we include the effect of non-zero Görtler number (Ge). This only modifies the $y-$ momentum equation given

by Tumin .[17] The governing equations in are given as,

$$(A\phi)_x = B_0\phi + B_1\phi_y + B_2\phi_{yy} \tag{18}$$

Comparing with Eq. 18 with Eq. 6, we find

$$\begin{aligned} \mathcal{A} &= A \\ \mathcal{B}_1 &= B_1 \\ \mathcal{B}_2 &= B_2 \\ \mathcal{B}_0 &= B_0 + G \end{aligned} \tag{19}$$

Here, G accounts for the contribution coming from the non-zero Görtler number. The non-zero entries of G are given as

$$\begin{aligned} G^{31} &= -2Ge^2\bar{\rho}\bar{U} \\ G^{34} &= Ge^2\bar{\rho}^2\bar{U} \end{aligned} \tag{20}$$

Acknowledgments

This work was sponsored by Air Force Office of Scientific Research under grant number FA9550-12-1-0064 and the Office of Naval Research under grant number N00014-15-1-2522. The views and conclusions contained herein are those of the authors and should not be interpreted as necessarily representing the official policies or endorsements, either expressed or implied, of the funding agencies or the U.S. Government.

References

[1]Benay, R., Chanetz, B., Mangin, B., Vandomme, L. and Parraud, J., "Shock wave/transitional boundary layer interactions in hypersonic flow.", *AIAA J.*, Vol. 44, No. 6, pp. 1243-1254.

[2]Bleibens, M. and Olivier, H., "On the influence of elevated surface temperatures on hypersonic shock wave/boundary layer interaction at a heated ramp model," *Shock Waves*, Vol. 15, 2006, pp. 301-312

[3]Cossu, C., Chomaz, J.-M., Huerre P. and Costa M., "Maximum spatial growth of Görtler vortices," *Flow, Turbulence and Combustion*, Vol. 65, 2000, pp. 369-392

[4]Ganapathisubramani, B., Clemens, N. T., and Dolling, D. S., "Effects of upstream boundary layer on the unsteadiness of shock-induced separation," *Journal of Fluid Mechanics*, Vol. 585, 2007, pp. 369-394.

[5]Shrestha, P., Dwivedi, A., Hildebrand, N.J., Nichols, Joseph W., Jovanovic, Mihailo R., and Candler, Graham V.,"Interaction of an oblique shock with a transitional Mach 5.92 boundary layer", 46th AIAA Fluid Dynamics Conference, 2016, Washington D.C.

[6]Wu, M. and Martin, M. P., "Direct numerical simulation of supersonic turbulent boundary layer over a compression ramp," *AIAA Journal*, Vol. 45, No. 4, 2007, pp. 879-889.

[7]Robinet, J.-Ch., "Bifurcations in shock-wave/laminar-boundary-layer interaction: global instability approach," *Journal of Fluid Mechanics*, Vol. 579, 2007, pp. 85-112.

[8]Guiho, F., Alizard, F., and Robinet, J.-Ch.,"Instabilities in oblique shock wave/laminar boundary-layer interactions," *Journal of Fluid Mechanics*, Vol. 789, 2016, pp. 1-35.

[9]Pagella, A., Rist, U., and Wagner, S., "Numerical investigations of small-amplitude disturbances in a boundary layer with impinging shock wave at Ma=4.8," *Physics of Fluids*, Vol. 14, No. 7, 2002, pp. 2088-2101.

[10]Clemens, N. T. and Narayanaswamy, V., "Low-frequency unsteadiness of shock wave/turbulent boundary layer interactions," *Annual Review of Fluid Mechanics*, Vol. 46, 2014, pp. 469-492.

[11]Sandham, N. D., Schülein, E., Wagner, A., Willems, S., and Steelant, J., "Transitional shock-wave/boundary-layer interactions in hypersonic flow," *Journal of Fluid Mechanics*, Vol. 752, 2014, pp. 349-382.

[12]Martin, M.P., Priebe, S., and Helm, C.M.,"Upstream and Downstream Influence on STBLI Instability," 46th AIAA Fluid Dynamics Conference, 2016, Washington D.C.

[13]Schmid, P. J., and Henningson, Dan S.,"Stability and Transition in Shear Flows," Springer, 2000

[14]Schmid, P. J.,"Non-modal Stability Theory,"*Annual Review of Fluid Mechanics*, Vol. 39, 2007, pp. 129-162

[15]Schülein, E.,"Effects of Laminar-Turbulent Transition on the Shock-Wave/Boundary-Layer Interaction," 44th AIAA Fluid Dynamics Conference, Atlanta, GA, 2014.

[16]Anderson, P. , Berggren, M. , and Henningson, D. S.,"Optimal disturbances and bypass transition in boundary layers,"*Physics of Fluids*, Vol. 11, No.1, 1999, pp. 134-150

[17]Tumin, A., and Reshotko, E.,"Optimal Disturbances in Compressible Boundary Layers,"*AIAA Journal*, Vol.41, No.12, 2003, pp. 2357-2363

[18]Pralits, J. O., Airiau C., Hanifi, A., and Henningson, D. S.,"Sensitivity Analysis Using Adjoint Parabolized Stability Equations for Compressible Flows," *Flow, Turbulence and Combustion*, Vol. 65, 2000, pp. 321-346

[19]Marxen, O., Lang, M., Rist, U., Levin, O., and Henningson, D. S.,"Mechanism for spatial steady three-dimensional disturbance growth in a non-parallel separating boundary layer," *Journal of Fluid Mechanics*, Vol. 634, 2009, pp. 165-189.

[20]Subbareddy, P. K. and Candler, G. V., "A fully discrete, kinetic energy consistent finite-volume scheme for compressible flows," *Journal of Computational Physics*, Vol. 228, No. 5, 2009, pp. 1347-1364.

[21]Ducros, F., Ferrand, V., Nicoud, F., Weber, C., Darracq, D., Gacherieu, C., and Poinsot, T., "Large-eddy simulation of the shock/turbulence interaction," *Journal of Computational Physics*, Vol. 152, No. 2, 1999, pp. 517-549

[22]Semper, M. T., Pruski, B. J., and Bowersox, R. D. W., "Freestream turbulence measurements in a continuously variable hypersonic wind tunnel," AIAA Paper No. 2012-0732, June 2012, pp. 1-13.

[23]M. R. Jovanović, "Modeling, analysis, and control of spatially distributed systems," *PHD thesis, University of California, Santa Barbara*, 2004

[24]M. R. Jovanović and B. Bamieh, "Componentwise energy amplification in channel flows," *J. Fluid Mech.*, Vol. 534, 2005, pp. 145-183

[25]Wright, M. J., Candler, G. V., and Prampolini, M., "Data-Parallel Lower Upper Relaxation Method for the NavierStokes Equations," *AIAA Journal*, Vol. 34, No. 7, 1996, pp. 1371-1377.

[26]Nompelis, Ioannis, Drayna, Travis W., Candler, Graham V., "Development of a Hybrid Unstructured Implicit Solver for the Simulation of Reacting Flows Over Complex Geometries," 34th AIAA Fluid Dynamics Conference and Exhibit, Portland, Oregon, 2004.

[27]Kendall, J. M., "Wind-tunnel experiment relating to the supersonic and hypersonic boundary layer transition," *AIAA J.*, vol. 13, No. 3, pp. 290-299.

[28]Loginov, M. S., Adams, N. A., Zheltovodov A. A., "Large-eddy simulation of shock-wave/turbulent-boundary-layer interaction", *J. Fluid Mech.*, vol. 565, 2006, pp. 135169

[29]Hall, P., "The linear development of Görtler vortices in growing boundary layers," *J. Fluid Mech.*, Vol. 130, 1983, pp. 41-58

[30]Luchini, P., "Reynolds number independent instability of boundary layer over a flat surface Part 2: optimal perturbations," *J. Fluid Mech.*, vol. 404, 2000, pp. 289-309

[31]Malik, M. R., "Numerical Methods for Hypersonic Boundary Layer Stability," *Journal of Computational Physics*,Vol. 86, 1990, pp. 376-413.

[32]Mack, L.M.,"Boundary Layer Stability Theory," Jet Propulsion Lab., JPL Rept. 900-277, California Inst. of Technology, Pasadena, CA, Nov. 1969

[33]Martinez, S. Navarro and Tutty, O. R., "Numerical simulation of Görtler vortices in hypersonic compression ramps," *Computers & Fluids*, Vol. 34, 2005, pp. 225-247

[34]Heffner, K. S., Chpoun, A., Lengrand, J. C., "Experimental investigations of transitional axisymmetic shock-boundary layer interactions at Mach 5," AIAA Paper, 93-3131, 1993

[35]Hakkinen, R. J., Greber, I., Trilling, L. and Abarbanel, S. S., "The interaction of an oblique shock wave with a laminar boundary layer," *Tech. Rep.* 2-18-59W. NASA Memo (1959)

[36]Hanifi, A.,Schmid, P.J.,and Henningson, D.S.,"Transient Growth in Compressible Boundary Layer Flow," Physics of Fluids, Vol. 8, 1996, pp. 51-65

[37]Reshotko, E., "Transient growth: a factor in bypass transition," *Phys. Fluids*, Vol. 13, 2001, No. 5, pp. 1067-1075

[38]Stewartson, K. and Williams, P. W., "Self-induced separation," *Proc. R. Soc. Lond.* A, Vol. 312, 1969, No. 1509, pp. 181-206

[39]Wagner, A., Kuhn, M., Schramm, J. M. and Hannemann, K., "Experiments on passive hypersonic boundary layer control using ultrasonically absorbtive carbon-carbon material with random microstructure," *Exp. Fluids*, Vol. 54, 2013, No. 10, pp 1606

[40]Yang, L., Zare-Behtash, H., Erdem, E. and Kontis, K., "Investigation of double ramp in hypersonic flow using luminescent measurement systems," *Experimental Thermal and Fluid Science*, Vol. 40, 2012, pp. 50-56

[41]Yao, Y., Krishnan, L., Sandham, N. L. and Roberts, G. T., "Effect of Mach number on unstable disturbances in shock/boundary-layer interactions," *Phys. Fluids*, Vol. 19, 2007, 054104

[42]Ehrenstein, U. and Gallaire, F., "Two-dimensional global low-frequency oscillations in a separating boundary-layer flow," *J. Fluid Mech.*, Vol. 614, 2008, pp. 315-327

[43]Rodrguez, D., Gennaro, E. M. and Juniper, M. P.,"The two classes of primary modal instability in laminar separation bubbles," *J. of Fluid Mech.*, Vol. 734, 2013, pp. R4:1-11

[44]Rodriguez, D. and Theofilis, V."Structural changes of laminar separation bubbles induced by global linear instability," *J. of Fluid Mech.*, Vol. 655, 2010, pp. 280-305

[45]Theofilis, V., Hein, S. and Dallmann, U., "On the origins of unsteadiness and three-dimensionality in a laminar separation bubble," *Philosophyical Transac. of the Royal Society*, Vol. 358, 2000, No. 1777, pp. 3229-3246